

Influence of Frequency Response Analysis on MH-47G DAFCS Development and Flight Test

Douglas W. Link

Boeing Rotorcraft, Philadelphia, PA

Bryan E. Kashawlic

Boeing Rotorcraft, Philadelphia, PA

Brian T. Fujizawa

US Army Aeroflightdynamics Directorate, Moffett Field, CA

Mark B. Tischler

US Army Aeroflightdynamics Directorate, Moffett Field, CA

ABSTRACT

Frequency domain design techniques are a very important element of designing good control laws and are widely used for rotorcraft control system development. This paper discusses how frequency response analysis was specifically applied to the MH-47G Digital Automatic Flight Control System (DAFCS) and how the results of the analysis impacted both flight test methodologies and the final control system design. Topics such as system identification, stability robustness, and disturbance rejection are all discussed along with specific examples of the challenges encountered when determining their quantitative values. Examples include assigning an accurate describing function for a non-linear algorithm inside of the control system, while another is identifying an open-loop response by using a closed-loop response. The paper concludes with a brief discussion of how frequency sweep injection locations can affect both the nature and accuracy of the frequency response. This paper is suited for those with a working knowledge of linear analysis, aircraft handling qualities, and control system design.

Nomenclature

| | | | |
|-------------------|--|----------------------|---|
| \bar{A}^C | body axis acceleration vector at aircraft CG | δ_b | longitudinal stick perturbation |
| \bar{A}^E | sensed body axis acceleration vector at EGI | δ_c | collective arm perturbation |
| M_{RL} | magnitude of rate limit | δ_r | directional pedal perturbation |
| P | body axis roll rate | δ_s | lateral stick perturbation |
| q | body axis pitch rate | ΔT | time step |
| r | body axis yaw rate | ϕ_D | steady state rate limiter phase delay |
| \bar{R}^{CE} | position vector from aircraft CG to EGI | θ | aircraft pitch angle |
| u | body axis longitudinal velocity | ϕ | aircraft bank angle |
| v | body axis lateral velocity | ψ | aircraft heading |
| $\dot{\bar{V}}^C$ | body axis velocity vector time derivative at aircraft CG | ${}^e\dot{\omega}^u$ | body axis angular velocity vector time derivative |
| \bar{V}^C | body axis velocity vector at aircraft CG | ${}^e\bar{\omega}^u$ | body axis angular velocity vector |
| \bar{V}_0^C | body axis velocity vector at aircraft CG (initial) | ω | frequency (rps) |
| \bar{V}^E | sensed body axis velocity vector at EGI | | |
| w | body axis normal velocity | | |

Introduction

The primary development phase of the MH-47G DAFCS (Digital Automatic Flight Control System) program started in the beginning of 2009 as part of a CRADA (Cooperative Research and Development Agreement) between the United States Army and Boeing [1]. Frequency response analysis was one of the major components of work that was performed during the program's developmental and two flight test phases. The paper discusses how frequency response analysis was used in system identification, control law design, and the determination of system performance and stability robustness.

During the first test phase, taking place in early 2009, pilot-generated frequency sweeps were flown on an MH-47G equipped with an analog AFCS for the purposes of plant identification. Through the use of CIPHER®, state space models of the MH-47G airframe were identified and compared to the non-linear Boeing Helicopter Simulation model (BHSIM) [2]. Once verified, the identified models were implemented in a Simulink® model, which included linearized versions of the developmental control laws as part of a CONDUIT® problem for the purposes of evaluating various ADS-33 specifications. Prior to the identification of CIPHER® aircraft models, the Simulink® model was run using aircraft models generated from Boeing's non-linear flight dynamics code – M97. Figure 1 shows a top level diagram of the Simulink® model used in the CONDUIT® problem [3]. In addition to the linearized developmental control laws (DAFCS), linear actuator models for the lower-stage flight controls are incorporated into the Simulink model to provide inputs into the M97 and CIPHER® models which include the upper-stage flight controls, plant, and sensor dynamics.

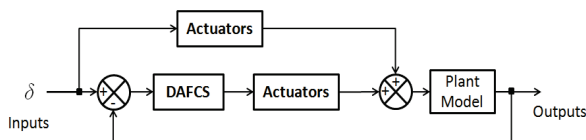


Figure 1: Top-Level Simulink® Model used in CONDUIT® Problem

Figure 2 shows a comparison of directional axis step responses among flight data, BHSIM, and the Simulink® model which is based on the identified CIPHER® aircraft models for the MH-47G airframe. The figure shows that the directional axis closed-loop plant dynamics are modeled accurately between the actual aircraft and the two models. This is important as the overall purpose of the linear analysis performed on this program was to make predictions about design changes and from the identified models and verify them using flight test data during phase II flight testing.

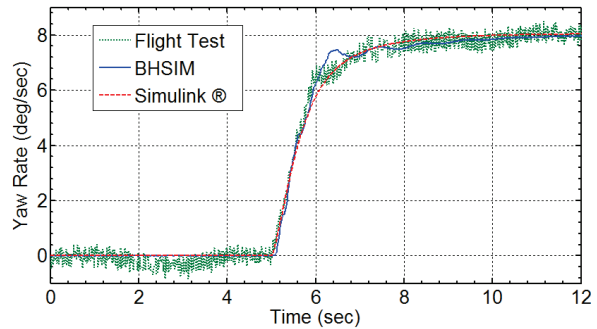


Figure 2: Comparison of Directional Axis Step Responses (Hover Condition)

Prior to the second phase of flight testing, various control law configurations had been evaluated in Boeing's non-linear pilot-in-the-loop simulation lab and fine-tuned in order to determine the configuration that would be used for first flight. During this phase of flight testing, occurring throughout the middle of 2010, frequency response analysis was used for the purposes of tuning and evaluating changes to DAFCS control law parameters. Unlike the first phase of data gathering, frequency sweeps were generated from the Flight Test Interface Panel (FTIP – see Figure 3) at summing locations inside of the DAFCS control laws where they were injected as disturbance inputs (Figure 17). With proper instrumentation, these types of frequency sweeps provide a means for the simple and accurate identification of disturbance rejection characteristics and stability margins. Because data collection was performed with stability augmentation on, additional calculations were performed using MATLAB® to extract the open-loop response.



Figure 3: Flight Test Interface Panel

MH-47G Plant Identification

Phase I Flight Testing:

The collection of test points needed to perform accurate plant identification was one of the largest sections of the first phase flight testing plan. One of the reasons for this was the need to identify plant models at six different configurations (variations of airspeed and gross weight). Data was collected in hover, 60 kts, and 110 kts at both 35,000 lbs and 46,000 lbs. A typical flight, for the purposes of plant identification, began by gathering trim data which was then followed by two pilot-generated frequency sweeps and doublets (starting in opposite directions) in each axis. Following the guidance of Tischler and Remple, each of the frequency sweeps lasted approximately 2 minutes and excited frequencies in the range of 0.05Hz to 2.0Hz (1.5 Hz in yaw and collective axes)^[2]. In order to aid the pilot in performing frequency sweeps, both visual and aural cueing was provided by a personal digital assistant.

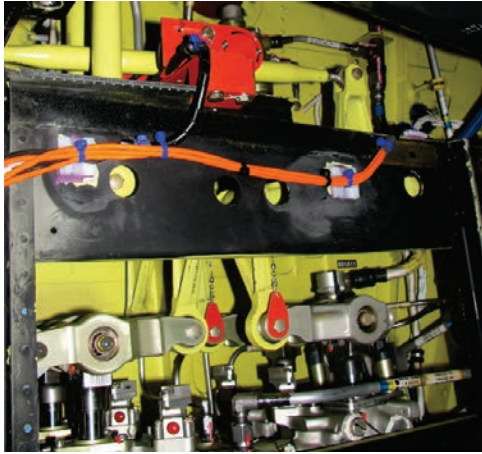


Figure 4: Mixer Input String Potentiometers

String potentiometers were attached to the flight controls at the input to the controls mixer in each axis as shown above Figure 4. At this location in the flight controls (see Figure 5), both the pilot and AFCS contributions have been summed together and subjected to the actuator dynamics in the lower flight controls. This is a very important point for air-frame ID as this signal constitutes the total input to the aircraft in a particular axis; therefore it must be known accurately from direct flight-test measurements.

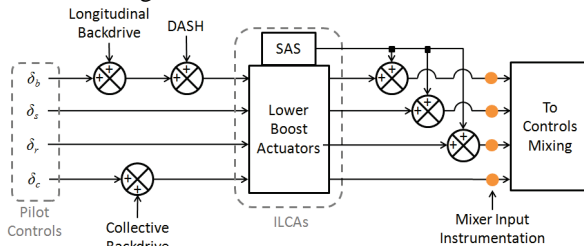


Figure 5: MH-47G Lower Stage Flight Controls

While the instrumented mixer inputs can be synthesized by summing and filtering the individual actuator positions, the inputs used for the plant identification were the instrumented mixer signals themselves because they are a more direct measurement of the control input transmitted to the swashplate. In addition, this choice of input also eliminates the need to model the lower boost actuator dynamics – which could introduce a source of error into the plant identification.

Aircraft state data were obtained from two EGI (Embedded GPS and INS) sensors. Angular and linear rates, Euler attitudes, and linear accelerations were all obtained from these two sensors. While a variety of other signals were available, the aircraft states and the mixer inputs were the only pieces of data needed to perform plant identification.

Data Processing:

Flight data were downloaded and formatted for use into MATLAB[®]. Once the data were imported to MATLAB[®], they were post-processed to be compatible with CIPHER[®]. One example of the additional post-processing required was the need to transform the velocities and accelerations from each EGI sensor location to the aircraft CG. Equations 1, 2, and 3 were applied to the EGI data in order to obtain the velocities, accelerations, and velocity time derivatives at the aircraft CG, respectively.

$$\vec{V}^C = \vec{V}^E - {}^e\vec{\omega}^u \times \vec{R}^{CE} \quad (1)$$

$$\vec{A}^C = \vec{A}^E - {}^e\dot{\vec{\omega}}^u \times \vec{R}^{CE} - {}^e\vec{\omega}^u \times ({}^e\vec{\omega}^u \times \vec{R}^{CE}) \quad (2)$$

$$\dot{\vec{V}}^C = \vec{A}^E - {}^e\dot{\vec{\omega}}^u \times \vec{R}^{CE} - {}^e\vec{\omega}^u \times \vec{V}^E + \vec{g} \quad (3)$$

After computing the transformed signals, a basic kinematic consistency check was performed by comparing the body axis velocity vector to the integrated body axis velocity vector time derivative and calculating an average error based on squared difference (see Equation 4). No objectionable differences were found in any of the individual vector components for the records used in the plant identification.

$$J = \frac{\sum_{n=1}^N \left[\sum_{k=1}^n \dot{\vec{V}}_k^C \Delta t - (\vec{V}_n^C - \vec{V}_0^C) \right]^2}{N} \quad (4)$$

Plant Identification Model Structure:

As shown in Figure 6, the MH-47G is a tandem configuration helicopter. Because of this, one of the assumptions made throughout the system identification was that the longitudinal/heave and lateral/directional axes are decoupled. The result is that many of the off-axis stability derivatives are eliminated from the identification and the complexity of the problem is significantly reduced.



Figure 6: MH-47G Test Aircraft M3763

As mentioned above, the longitudinal/heave and lateral/directional dynamics of the MH-47G airframe were identified separately. The state space model structures assigned for each pair of aircraft axes are given below by equations 5 (longitudinal/heave) and 6 (lateral/directional).

$$\begin{pmatrix} \dot{u} \\ \dot{w} \\ \dot{q} \\ \dot{\theta} \end{pmatrix} = \begin{bmatrix} X_u & X_w & X_q & -gc\theta_0 \\ Z_u & Z_w & Z_q + U_0 & 0 \\ M_u & M_w & M_q & 0 \\ 0 & 0 & 1 & 0 \end{bmatrix} \begin{pmatrix} u \\ w \\ q \\ \theta \end{pmatrix} + \begin{bmatrix} X_{\delta_b} & X_{\delta_c} \\ Z_{\delta_b} & Z_{\delta_c} \\ M_{\delta_b} & M_{\delta_c} \\ 0 & 0 \end{bmatrix} \begin{pmatrix} \delta_b \\ \delta_c \end{pmatrix} \quad (5)$$

$$\begin{pmatrix} \dot{v} \\ \dot{p} \\ \dot{r} \\ \dot{\phi} \end{pmatrix} = \begin{bmatrix} Y_v & Y_p & Y_r - U_0 & gc\phi_0 \\ L_v & L_p & L_r & 0 \\ N_v & N_p & N_r & 0 \\ 0 & 1 & 0 & 0 \end{bmatrix} \begin{pmatrix} v \\ p \\ r \\ \phi \end{pmatrix} + \begin{bmatrix} Y_{\delta_s} & Y_{\delta_r} \\ L_{\delta_s} & L_{\delta_r} \\ N_{\delta_s} & N_{\delta_r} \\ 0 & 0 \end{bmatrix} \begin{pmatrix} \delta_s \\ \delta_r \end{pmatrix} \quad (6)$$

During the identification process, several of the off-axis stability and control derivatives were eliminated. Additional biases, such as the U_0 term, were also implemented into the state space model for the forward flight configurations to properly separate out certain stability derivatives from the airframe's overall dynamic response. While not explicitly shown in equations 5 and 6, time delays were also identified in each axis in order to incorporate approximations of higher-order dynamics into the low-order state space models. After the parameters for a particular state space model were identified, independent flight test data was used to verify the accuracy of the identified state space models in the time domain.

Plant Identification Results:

In general, the identified state space models produced dynamic responses that matched independent flight test data well. An example is shown below in Figure 7 which highlights the response of a lateral doublet to various lateral/directional states for the 35,000 pound hover condition.

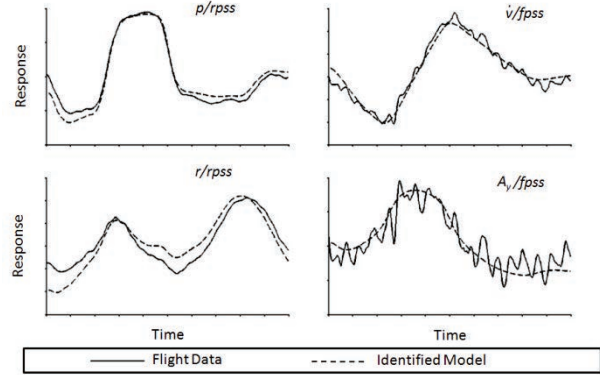


Figure 7: Time Domain Verification of Identified State Space Models (Lat/Dir - 35K Hover)

One of the direct benefits of identifying a low-order equivalent physical state space model is the ability to update control law parameters that utilize stability and control derivatives with more accurate estimates. The automatic trim algorithms utilized throughout DAFCS use the on-axis stability and control derivatives in order to estimate the total amount of control input required to trim the aircraft^[4]. If the \mathbf{A} and \mathbf{B} matrices in equation 7 are reduced to include the diagonal (on-axis) terms only, then solving this equation for u is the prediction for the additional amount of control required to trim the plant.

$$\dot{\bar{x}} = \mathbf{A}\bar{x} + \mathbf{B}\bar{u} \quad (7)$$

The values of the stability and control derivatives do not need to be exact in the expression above in order for the auto trim algorithms to work well because of the robustness inherent in the feedback control.

While the ability to fine tune parameters in the trim prediction algorithms was one advantage of identifying physical state space models, much more benefit was realized during the developmental phase occurring in between the MH-47G analog and digital flight test programs. During this phase, the models were used in order to tune various control law parameters in all aircraft axes, predict levels of ADS-33 handling qualities, and estimate stability and performance characteristics of the MH-47G equipped with DAFCS.

Frequency Response Analysis Before MH-47G Phase II Flight Testing

In between the two flight testing phases (occurring about 1 year apart), a significant amount of development work was performed to enhance the DAFCS control laws for the MH-47G. The longitudinal axis was re-tuned for improved attitude response and more precise airspeed hold. The directional axis was updated for enhanced turn coordination and trim management. Additional enhancements were incorporated into the lateral and vertical axes as well as the low speed regime modes. The remainder of this section will discuss some of the specific applications of frequency response analysis to each axis.

Longitudinal Axis:

One of the applications of frequency response analysis performed in the longitudinal axis was the sizing of the filter time constant which is used in the calculation of regulated pitch rate for coordinated turns (see Figure 8). In the analog MH-47G, this time constant was fixed at a relatively long two seconds. As shown in Figure 9, the benefit of having a longer time constant on this path is increased stability margins. However, if the aircraft is quickly rolled out of a turn back to level flight, the lagged $r \tan(\phi)$ term will momentarily still be contributing to the longitudinal axis AFCS command. The result of this is an undesirable tendency for the aircraft to momentarily pitch upwards.

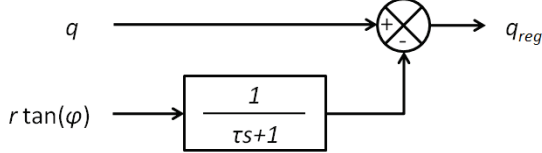


Figure 8: Calculation of Regulated Pitch Rate

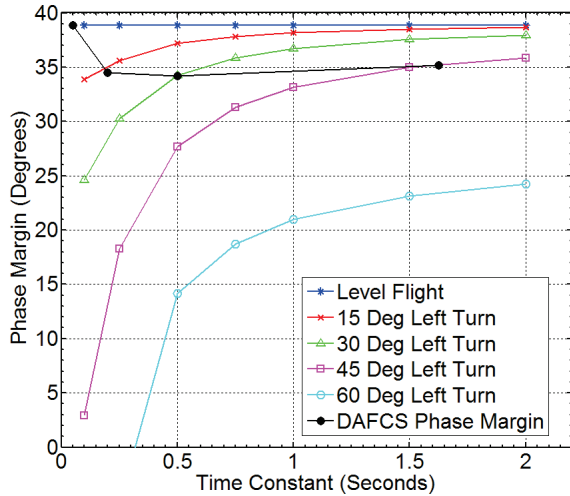


Figure 9: Relationship between Filter Time Constant (Regulated Pitch Rate) and Phase Margin

In order to reduce the pitch-up tendency when quickly rolling out of a turn, the lag filter time constant can be decreased at the cost of lower stability margins. By injecting frequency sweeps at various trimmed flight conditions (as a function of increasing bank angle) in the Simulink/CONDUIT[®] model, predicted stability margins were computed for each condition using the M97 plant models. CIPHER[®] models were not used for this analysis because no identification was performed in banked turns. The balance considered throughout the analysis was the trade-off in phase margin as a function of bank angle and lag filter time constant. As a result, the filter time constant was modified such that it was scheduled with bank angle. By choosing a smaller initial time constant that increases with bank angle, the tendency to pitch up after rapidly rolling to wings-level was eliminated with minimal impact to stability margins. Throughout the study, phase margin was more critical than gain margin (which remained relatively independent of bank angle), and left turns produced slightly lower margins than right turns. Figure 10 shows a comparison of the phase margin before and after the lag filter time constant architecture was modified to include a variable filter time constant.

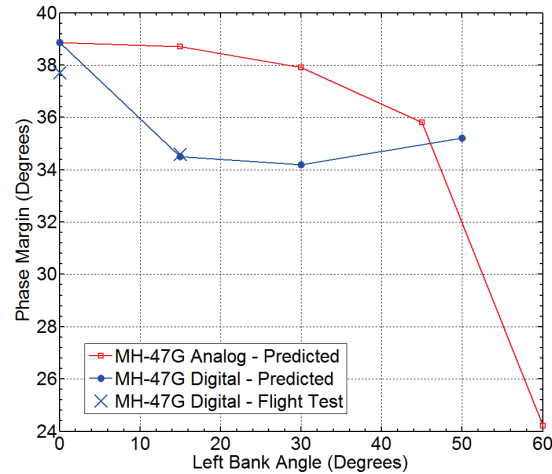


Figure 10: Comparison of Long Axis Phase Margin between Analog and Digital MH-47G Platforms

Another important aspect considered in the longitudinal axis during the development phase was the impact to piloted bandwidth as a result of the changes made. Utilizing BHSIM to generate and analyze frequency responses was efficient and effective; however additional modifications were necessary to the Simulink/CONDUIT[®] model in order to handle some of the non-linearities in the DAFCS controls laws. The most significant of these non-linearities is a moderately slow, but important, rate limit occurring in a portion of the longitudinal stick feed-forward path. The purpose of this rate limit is to allow high stick gains for airspeed stability while maintaining desirable levels of attitude sensitivity.

In order to more accurately capture the dynamics of the non-linear rate limit, a first order lag was used as a describing function. This type of implementation was selected because it is simple and it captures the steady state phase offset and magnitude attenuation caused by a non-linear, symmetric rate limiter. Figure 11 demonstrates this behavior showing a sinusoid with sufficient amplitude and frequency to exercise the specified rate limit magnitude. After just two full cycles, the transient response has settled and the phase delay between the input and output is constant.

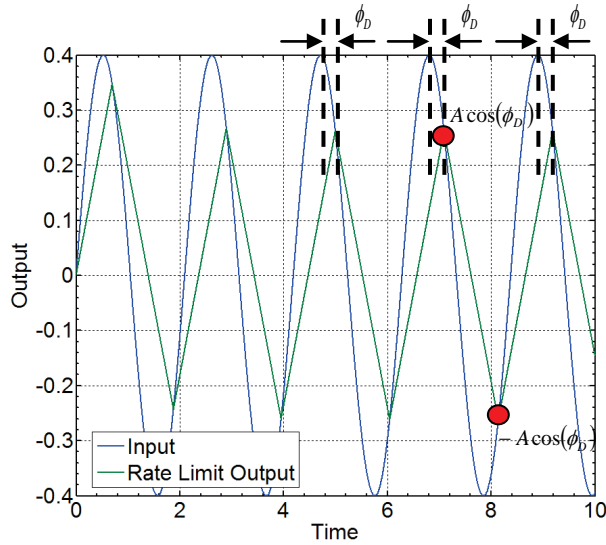


Figure 11: Behavior of Symmetric Rate Limit in Steady State Operation

Utilizing the qualitative behavior of the rate limit, as seen above in Figure 11, the phase delay between the input and output can be calculated in terms of the input amplitude (A), the input period (T), and the magnitude of the rate limit (M_{RL}) as expressed by equation 8. Note that if the quantity inside the inverse cosine function is greater than 1, the rate limit is never exercised for that particular input magnitude and frequency. In addition, the amount of phase lag incurred at a given frequency (or period) by a first order lag filter with bandwidth ω_L is given by equation 9.

$$\phi_D = \cos^{-1} \left[\frac{M_{RL}}{A} \left(\frac{T}{4} \right) \right] \quad (8)$$

$$\phi_L = \tan^{-1} \left(\frac{2\pi}{T\omega_L} \right) \quad (9)$$

By setting equations 8 and 9 to be equivalent, the lag filter bandwidth is determined by the simple relationship given in equation 10. Figure 12 demonstrates the lag filter approximation for the input shown above in Figure 11. Initially, this approximation has slight error near the first two local extrema, but the remainder of the rate-limited response is approximated

very well. Notice that by using the lag filter architecture with matched phase delay, the magnitude of the response is automatically satisfied.

$$\omega_L = \frac{2\pi}{T} \cot(\phi_D) \quad (10)$$

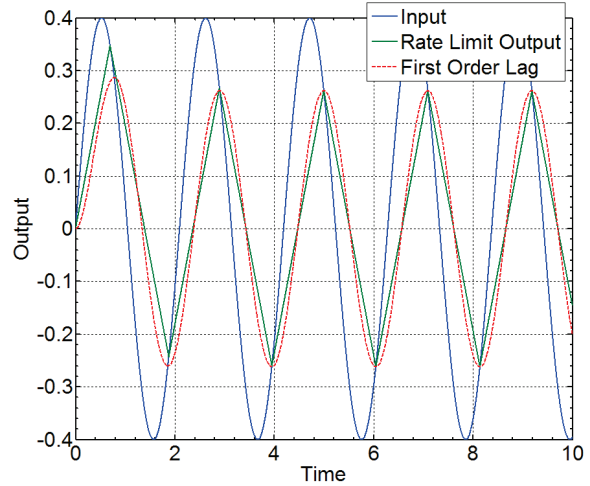


Figure 12: Lag Filter Approximation Of Symmetric Rate Limit

While this LTI (linear time invariant) approximation of a symmetric rate limit works well, the lag filter parameters are entirely dependent on the characteristics of the input. Increasing the magnitude or frequency of the input for a specified rate limit will reduce the lag filter bandwidth. Therefore, in order to build conservatism into the calculations used for piloted bandwidth, upper bounds for pilot input magnitude and frequency were used to quantify the rate limit approximation used in the Simulink/CONDUIT[®] model.

As well as approximating the rate limit as a lag filter, both extremes of modeling the rate limit as a unity gain and broken path were also investigated. Because the pitch axis core response type meets the character of ADS-33 ACAH (attitude-command attitude-hold), the piloted bandwidth is defined as the -135 degree phase crossing by ADS-33^[5]. One consequence of this is the non-intuitive result shown in Figure 13 which indicates that increased lag (lower filter bandwidth) in the rate limited feed-forward stick path increases the piloted bandwidth. This behavior is due to the delay caused by both the digital processing occurring in DAFCS and the DASH actuator dynamics which are relatively slow (2hz bandwidth). Phase-based bandwidth has no dependence on magnitude; therefore as the lag filter bandwidth approaches zero (broken path), a smaller portion of the combined mechanical input is from the DASH actuator containing the digital processing and actuator delays. The lag filter bandwidth of 2.23 rps is chosen by assuming an input with amplitude of 0.5 inches of stick at 0.4 Hz (approximately piloted bandwidth).

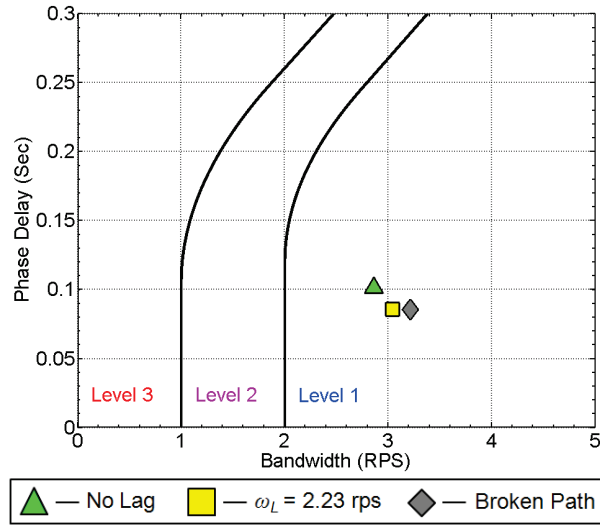


Figure 13: Effect of Rate Limit Approximations on Piloted Bandwidth (Long Axis - Hover)

During flight, the pilot is operating the aircraft between two extremes. Increased activity in the longitudinal stick moves the piloted bandwidth towards the gray diamond, while small, slow inputs shift the piloted bandwidth near the green triangle. In either case, the MH-47G has sufficient bandwidth and minimal phase delay for predicted level 1 handling qualities. Changes in flight condition or aircraft configuration do not significantly impact the bandwidth or delay characteristics.

Lateral Axis:

During the MH-47G DAFCS program, one of the new capabilities added to the lateral axis was the ability to select an ACAH response type in place of the traditional RCAH (Rate-Command Attitude-Hold) response type in forward flight [6]. This change was incorporated to enhance the handling qualities of the aircraft during aerial refueling tasks. Pilots commented that the aerial refueling task was easier to perform when using the ACAH response type when compared with the RCAH response type.

In order to quantify the benefit of the ACAH response type in the frequency domain, the Simulink/CONDUIT® model was updated to incorporate the necessary changes. Figure 14 shows the significant improvement to piloted bandwidth and phase delay (approximately 1.3 rps and 0.03 sec, respectively) when using an ACAH response type in place of RCAH. For a rate response type, the piloted bandwidth is determined as the lesser of the two definitions of bandwidth (phase-based and gain-based). In figure 14, the gain bandwidth is shown for the rate response type.

While the closed-loop characteristics of the frequency response are improved by switching from a rate response type to an attitude response type, there is no impact to the stability margins when switching between the two response types. No impact occurs in the stability margins because the differences between the ACAH and RCAH response types are entirely implemented by altering the feed forward control in the lateral stick pickoff path and reference bank angle computations, resulting in a near level 1 response for target acquisition and tracking.

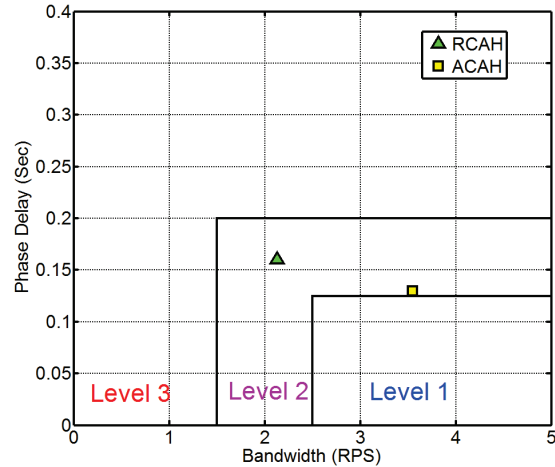


Figure 14: Piloted Bandwidth Comparison RCAH vs. ACAH (Lat Axis – 110 kts)

Another aspect that was investigated during the development phase was the consequence of utilizing fulltime auto-trim. Previously, auto trim was only used when the low speed VELSTAB (Velocity Stabilization) modes were active. Key frequency response metrics are compared in Table 1, and show minor sensitivity to many of the frequency response specs with the exception of a small loss in phase margin. Interestingly, the piloted bandwidth decreased for the rate response type when auto trim was enabled. The cause of this is due to a flat spot in the magnitude curve near the -180 phase crossing which reduces the gain-based bandwidth. Because the performance benefits of auto trim (including those not revealed by frequency responses) outweigh any of the adverse impacts to stability, the algorithm was enabled full-time in the lateral axis DAFCS control laws.

Table 1: Predicted Impact of Auto Trim on Frequency Response Specs (Lat Axis – 110 kts)

| Specification | Auto Trim Off | | Auto Trim On | |
|--------------------|---------------|------|--------------|------|
| | RCAH | ACAH | RCAH | ACAH |
| Gain Margin (dB) | 8.4 | | 8.0 | |
| Phase Margin (deg) | 38.7 | | 34.0 | |
| Dist Rej Bnw (rps) | 2.1 | | 2.1 | |
| Bandwidth (rps) | 2.6 | 3.3 | 2.1 | 3.5 |
| Phase Delay (sec) | 0.16 | 0.12 | 0.16 | 0.13 |

Directional Axis:

The directional axis was modified during the developmental phase of the GDAFCS program [7]. A yaw rate command model, automatic trim following, lateral acceleration feedback, and interfaces with the flight director were all implemented. Improvements were also made to turn coordination and moding logic, but the core feedback paths that use yaw rate and heading remained unchanged.

While the aircraft is operating in low speed mode (less than 40 knots airspeed), the turn coordination and lateral acceleration feedback modules are disabled. The result, from a frequency response perspective, is that the legacy and new directional axis control laws are identical with the exception of auto trim. Therefore, one way of validating the core feedback paths was to inject a frequency sweep with directional axis auto trim disabled and observe that the frequency responses between both the control laws were the same. This was performed in the Simulink/CONDUIT® and BHSIM models and the results confirmed that the legacy and new models' frequency responses matched with auto trim disabled. After confirming the models matched, auto trim was re-enabled and tuned based on both time domain and frequency domain analyses. The impact of auto trim in the directional axis from a frequency response perspective is shown in Table 2.

Table 2: Predicted Impact of Auto Trim on Frequency Response Specs (Dir Axis – Hover)

| Specification | Auto Trim Off | Auto Trim On |
|--------------------|---------------|--------------|
| Gain Margin (dB) | 14.8 | 10.6 |
| Phase Margin (deg) | 38.0 | 35.5 |
| Dist Rej Bnw (rps) | 1.1 | 1.2 |
| Bandwidth (rps) | 1.4 | 1.5 |
| Phase Delay (sec) | 0.13 | 0.11 |

Aside from using lateral acceleration feedback in place of sideslip feedback, the most significant change to the modules associated with turn coordination occurred in the proverse yaw feedback path (roll rate feedback into the directional axis). As shown in Figure 15, both the gain and lag filter time constant used in the feedback path were significantly reduced.

Additional tuning occurred during phase II flight testing; while changes to this feedback path were noticeable, significant improvement was observed during high-precision tasks such as HAR (Helicopter Aerial Refueling) or tasks requiring aggressive maneuvering (Slalom Mission Task Element). This is because the proverse yaw feedback path acts essentially as feed-forward control to match the yaw rate command

model. As a result, directional axis stability margins in forward flight are relatively insensitive to moderate changes in the proverse yaw feedback (see Figure 16), but aircraft bandwidth and responsiveness increase.

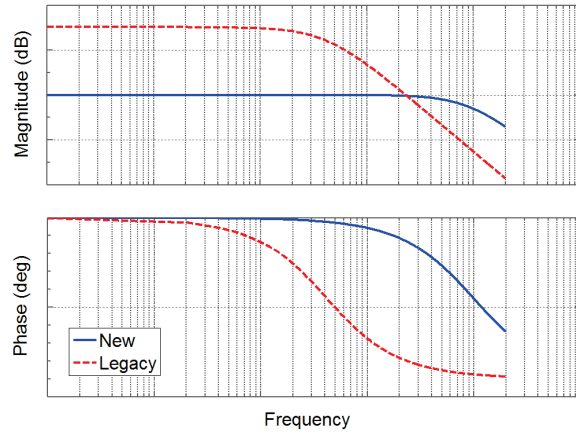


Figure 15: Comparison of Proverse Yaw Feedback Shaping (Forward Flight)

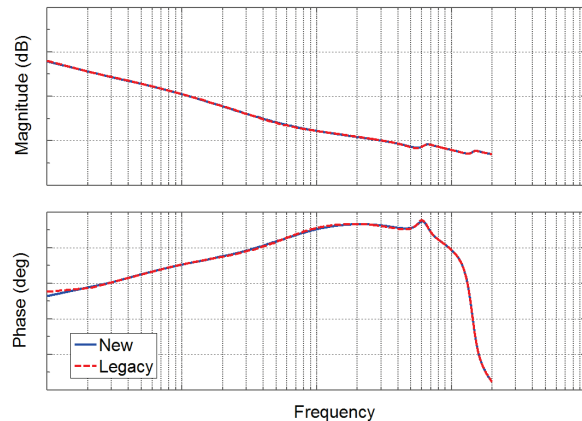


Figure 16: Proverse Yaw Feedback Impact on Directional Axis Open-Loop Frequency Response

Vertical Axis:

Other than changes to moding logic, no improvements were made to the vertical axis during the developmental phase. The reason is that the vertical axis is relatively simple; having only 3 major parts relevant to linear analysis: complementary filter on altitude, PI feedback on vertical velocity, and automatic trim following. In addition, because there is no vertical SAS (see Figure 5), all augmentation in the vertical axis is accomplished through the collective backdrive.

Frequency Response Analysis During MH-47G Phase II Flight Testing

During phase II flight testing, several gains in the longitudinal, lateral, and directional axes were tuned for improved handling qualities (only one parameter was changed in the vertical axes). Towards the end of phase II flight testing, computer-generated frequency sweeps were injected in each axis where they were observed by the AFCS as a control-equivalent disturbance as shown in Figure 17. The purpose of these sweeps was to quantify the stability and disturbance rejection characteristics of the aircraft, which would be compared with predictions to assess model accuracy and validity.

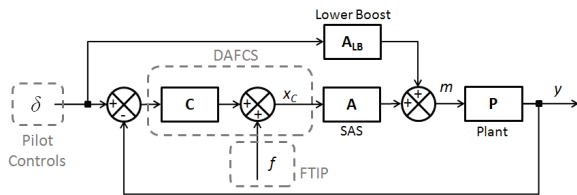


Figure 17: High Level Flight Controls / FTIP Configuration on MH-47G

Disturbance rejection characteristics can be determined by obtaining the transfer function from the FTIP input (f) to the total SAS command (x_c). Equation 11, which represents the algebra corresponding to the block diagram shown Figure 17, supports this statement; but it also indicates that the pilot controls must not be correlated to the FTIP sweep. Otherwise, the second term remains and more information must be known about the control system in order to compensate for this term. Because the pilot must not respond to the FTIP input in order to obtain useful data, a build up was done in each axis in order to ensure crew safety. With decent air quality, even frequency sweeps with a relatively small magnitude generated useful data.

$$\begin{pmatrix} x \\ f \end{pmatrix} = \underbrace{\begin{bmatrix} 1 \\ 1 + CPA \end{bmatrix}}_{\text{Sensitivity Function}} + \begin{bmatrix} C - CPA_{LB} \\ 1 + CPA \end{bmatrix} \begin{pmatrix} \delta \\ f \end{pmatrix} \quad (11)$$

If equation 11 is reduced to contain the first term only, then the open loop transfer function can be extracted from the closed loop response – this was the same method used in order to determine stability margins during the Comanche flight test program^[8]. Equation 12 shows the simple calculation required to do this. Note that $(x/f)^{-1}$ is not the same transfer function as (f/x) unless the coherence is identically 1.

$$G_{OL} = \left(\frac{x}{f} \right)^{-1} - 1 \quad (12)$$

Longitudinal Axis:

While this method for determining disturbance rejection characteristics and stability margins works well in the lateral, directional, and vertical axes; it requires slight modification in the longitudinal axis because the augmentation is split between the SAS portion of the ILCA (Integrated Lower Control Actuator) and the DASH (Differential AirSpeed Hold) actuator shown in Figure 18. Figure 19 shows the architecture of the flight controls specific to the longitudinal axis with the longitudinal backdrive removed (for simplicity).

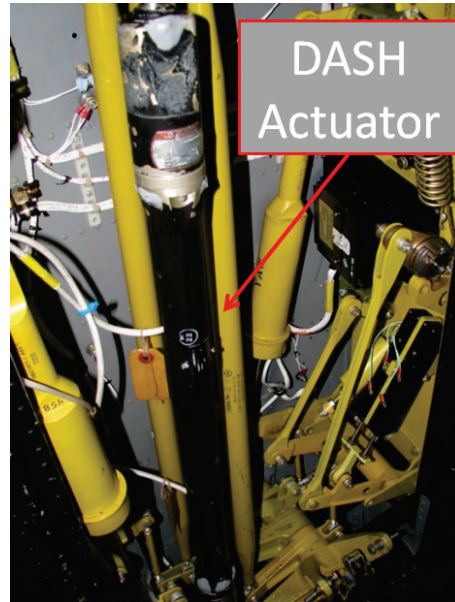


**Figure 18: DASH Actuator
(Linear Extensible Actuator with 2 Ends)**

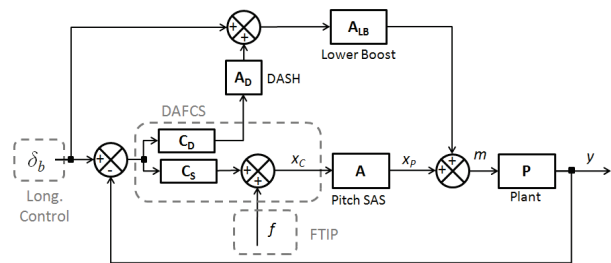


Figure 19: Longitudinal Axis Flight Controls

In order to account for all the augmentation provided by DAFCS, the output location must be moved to the pitch mixer (m). However, the consequence of this is that the FTIP input now includes the dynamics of the pitch SAS as indicated in equation 13 (which assumes the pilot control is not correlated with the FTIP input).

$$\begin{pmatrix} m \\ f \end{pmatrix} = \frac{A}{1 + CPA} \quad (13)$$

This equation can be re-written in terms of the transfer function between the SAS command and SAS position. Furthermore, because the coherence is near 1 when the frequency response is linear, the inverse SAS dynamics can be accurately obtained by taking the transfer function from the SAS position to the SAS command. The result is that the disturbance rejection characteristics can be obtained by taking the product of these two transfer functions as shown by equation 14. Similarly, the open loop transfer function can be obtained from the inverse closed loop response cascaded with the SAS dynamics (equation 15).

$$\left(\frac{m}{f}\right)\left(\frac{x_c}{x_p}\right) = \frac{1}{1 + CPA} \quad (14)$$

$$G_{OL} = \left(\frac{x_p}{x_c}\right)\left(\frac{m}{f}\right)^{-1} - 1 \quad (15)$$

Even if the longitudinal backdrive was enabled, its compensation would be included in the mixer input (just like the DASH). In general, this method can be applied as long as the FTIP input only goes through a single control path and the signal corresponding to the total amount of control transmitted to the airframe is available.

Figure 20 shows the frequency response of the pitch SAS. Both the frequency response from the command to its position and the inverse of its position to the command are shown. Once again, these frequency responses are nearly identical because the coherence is very close to 1. The actuator is relatively fast and exhibits little change in magnitude over the frequency region of interest. However, if unaccounted for, the phase loss incurred by not accounting for the actuator degrades the apparent stability margins by several degrees. Disturbance rejection characteristics are not significantly affected by neglecting the SAS dynamics because those specifications are dependent on the magnitude response only.

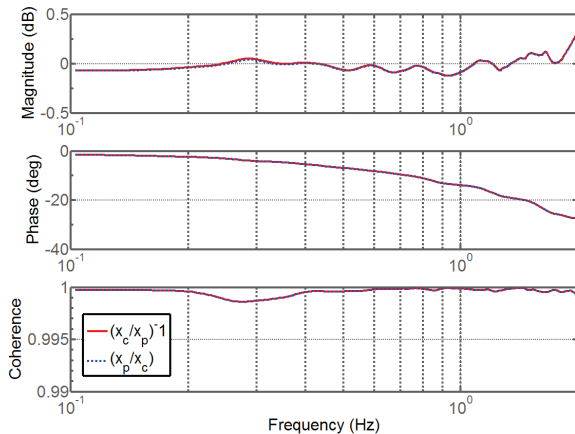


Figure 20: Pitch SAS Frequency Response (0.1-2 Hz)

Lateral Axis:

While hovering approximately below 25 feet above ground level with position hold mode engaged, pilots noticed slight, abrupt motion in the lateral axis referred to as “lateral darting.” Traditionally, the only additional compensation provided by position hold was proportional-integral inertial velocity feedback [9] [10]. In order to mitigate this undesirable motion, additional compensation was enabled in the form of inertial lateral acceleration feedback.

As shown in Figures 21 and 22, slightly increasing the inertial lateral acceleration feedback gain improves the disturbance rejection characteristics. This, however, comes at the expense of moderate losses in phase margin, and degraded disturbance rejection if the gain is increased too much. Moderate increases in the gain reduce overshoot in the bank angle response, but large increases in the gain cause undesirable activity in the response.

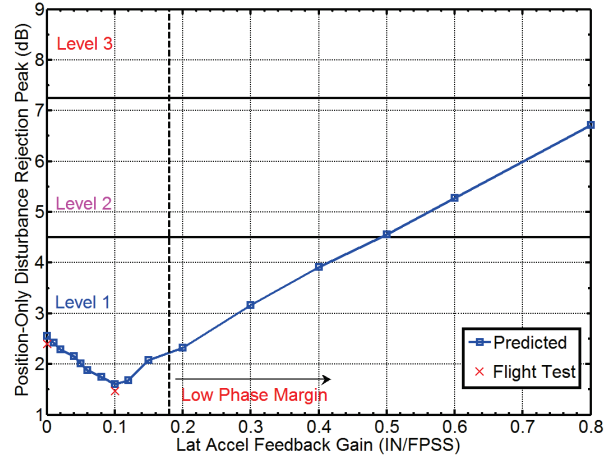


Figure 21: Impact of Lat Accel Feedback Gain to Position Disturbance Rejection Characteristics

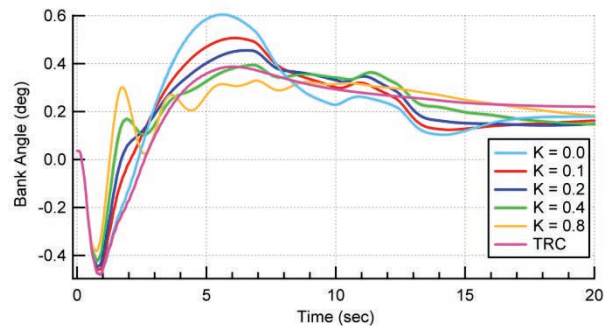


Figure 22: Bank Angle Response to Lateral Gust

Following the analysis shown above, test points were flown with inertial lateral acceleration feedback enabled. Data extracted from flight test agreed with pilot comments in that there was benefit to enabling a small amount of lateral acceleration feedback while ground speed augmentation is active.

Directional & Vertical Axes:

Towards the end of phase II flight testing, frequency sweeps were performed in each axis. As result of these sweeps, both the directional and vertical axes were found to have moderately large stability margins both in a hover and in forward flight. Test points were added to the flight cards in order to determine the effects of small alterations to feedback paths in these axes.

During the hover MTE (Mission Task Element), pilots noticed lateral movement of the visual reference with respect to the rectangular box (indicating the bounds for desired performance) as shown in Figure 23. Given this observation along with moderate amounts of stability margin in the directional axis, the lag filter time constant in the heading hold feedback path was reduced to its smallest adjustable value ($1/50^{\text{th}}$ second). When compared with nominal hover performance, pilots commented that they felt less lateral motion in the seat as a result of tightened yaw rate control.



Figure 23: Hover Board and Reference Symbol Used in Hover MTE

Figure 24, shows the impact of reducing the heading hold feedback lag filter time constant on directional axis stability margins as predicted by BHSIM. Actual margins are not shown because no sweeps were flown with the reduced lag filter time constant. Gain margin is affected more for low-speed conditions while phase margin is affected more for forward-flight conditions. Note that BHSIM is conservative in its ability to predict directional axis phase margins due to slight oversensitivity in the model at low frequency. Closed loop frequency responses are insensitive to changes in the heading hold feedback path because any intentional pilot inputs to the pedals will synchronize the heading reference – effectively disabling heading hold feedback.

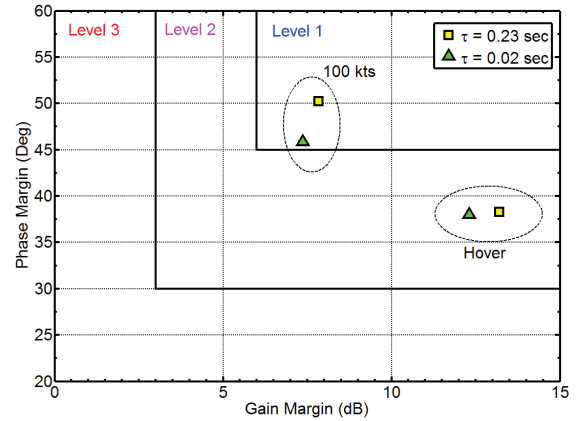


Figure 24: Impact of Heading Hold Feedback Lag Filter Time Constant on Dir Axis Stability

In the vertical axis, the impact of increasing the vertical velocity and altitude error gains were assessed along with reductions to the auto trim lag filter time constant. The purpose of these modifications was to improve the disturbance rejection characteristics at the expense of a portion of the excess stability margins. While increases to the feedback gains and auto trim bandwidth generally improved performance, the increased activity was also felt by the pilot because the only actuator that provides feedback in the vertical axis is the collective backdrive (which is configured in parallel with the collective arm).

Originally, it was believed that the relatively slow dynamics of the collective backdrive would not allow the actuator to respond too quickly to the AFCS commands. However, in response to pilot comments, a frequency sweep was injected into a collective backdrive actuator in a lab environment and a more accurate model was identified as shown in Figure 25.

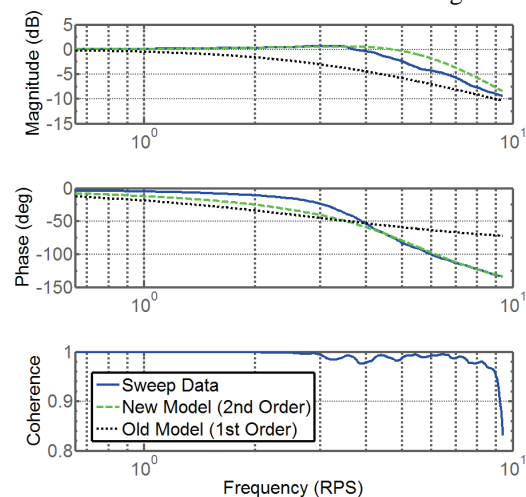


Figure 25: Collective Backdrive Actuator Frequency Response and Low-order Equivalent Models

The frequency sweeps indicated that the existing first-order model under-predicted the actuator bandwidth. One consequence of this was a built-in design margin which would cause optimization algorithms to tune feedback gains conservatively. As result of the identification, larger stability margins, which matched the flight test identified margins more closely, were predicted by the Simulink/CONDUIT® model. Additional tuning in flight test resulted in increasing the vertical velocity feedback gain only. The result was better disturbance rejection characteristics while maintaining desirable stability margins and predictable, non-excessive motion in the collective arm.

Remarks about FTIP Frequency Sweeps:

Throughout phase II flight testing, the ability to inject disturbances into the airframe was limited by the locations at which FTIP inputs could be summed into the existing AFCS commands. Therefore, all disturbances injected into the system would be observed by the plant as a force or moment, which would produce kinematically consistent observable states. The following discussion outlines how the location of the disturbance input can affect the perceived results of the disturbance rejection frequency response.

Assuming feedback was only performed on two dependent states (such as an attitude and its rate), then for a disturbance that is injected in terms of equivalent inches of control to a single actuator, the system is modeled by the diagram presented in Figure 26. In this diagram, the controller is divided into two independent parts which provide state feedback on individual plant states. The transfer function, in order to determine the disturbance rejection characteristics, is given by equation 16 which represents the sensitivity function, S (not to be confused with the Laplace variable s) [11]. Note that in this configuration, all of the observed states will include the effects of the disturbance and will be kinematically consistent.

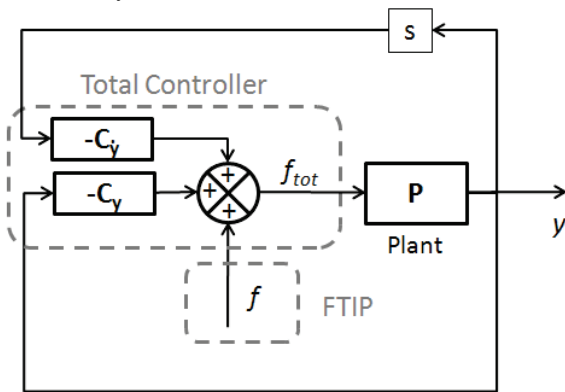


Figure 26: Disturbance Rejection Architecture (Control Equivalent Disturbance)

$$\frac{f_{tot}}{f} = \frac{1}{1 + (C_y + sC_{\dot{y}})P} = S \quad (16)$$

Another possible architecture for evaluating disturbance rejection is that shown in Figure 27. The major difference in this configuration is that the actual output states are not directly disturbed. Rather, the sensed states are disturbed which, in turn, causes the control system to respond. An example of this would be disturbances to radar altitude as result of tall objects moving on the ground. Furthermore, if the disturbance is injected in a manner that is kinematically inconsistent, then the apparent disturbance rejection characteristics will be altered by the effects of kinematic inconsistencies as outlined by equation 17.

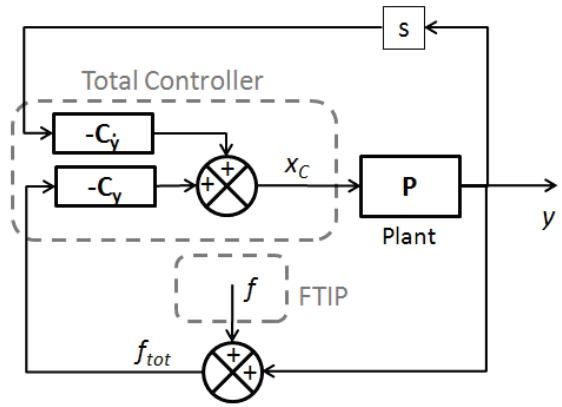


Figure 27: Disturbance Rejection Architecture (Attitude-only Equivalent Disturbance)

$$\frac{f_{tot}}{f} = G_{DRB} = \frac{1 + sC_{\dot{y}}P}{1 + \underbrace{(C_y + sC_{\dot{y}})P}_{\text{Total Controller}}} = S \underbrace{(1 + sC_{\dot{y}}P)}_{\text{Extra Term}} \quad (17)$$

The frequency response of the extra term appearing in equation 17 represents the loop transfer function if the only feedback path enabled in the architecture shown above was the rate feedback. While this frequency response may include higher-order dynamics, its magnitude will generally remain constant at low frequency and decrease to negligible values at high frequency. In cascade with the Laplace variable, s , the result will be a frequency response with an increase in magnitude throughout the mid-range frequency region.

Figure 28 provides an example of the behavior discussed above with specific application to the vertical axis. In the first case, the disturbance is injected as a control equivalent input; but in the second case it is injected as an altitude error only. The difference in the responses is very apparent as the kinematic inconsistencies decrease the -3dB crossing frequency (which is used in order to determine the disturbance rejection bandwidth in the pitch, roll, and yaw axes) [12].

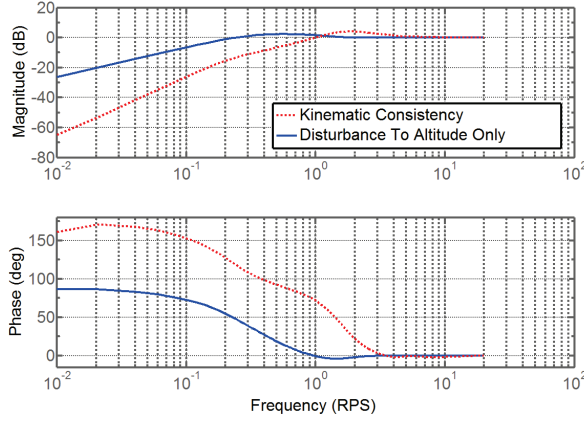


Figure 28: Predicted Disturbance Rejection Characteristics (Vertical Axis – 100 kts)

The frequency response bandwidths (defined as -3dB crossing frequency) and peaks (maximum magnitude) for each disturbance input configuration are presented below in Table 3. Note that there is no ADS-33 specification for disturbance rejection bandwidth/peak in the vertical axis. Therefore, the numbers presented are not technically defined as the disturbance rejection bandwidth/peak. However, the numbers presented are calculated based on the same principals, and can be used as a guideline in the determination of a formal disturbance rejection specification used by the vertical axis.

| Configuration | Value | |
|------------------------------------|-----------------|-----------|
| | Bandwidth (rps) | Peak (dB) |
| Control equivalent disturbance | 0.75 | 4.0 |
| Altitude disturbance only (ADS-33) | 0.15 | 2.3 |

Table 3: Disturbance Rejection Bandwidths and Peaks Obtained From Figure 28

If higher order state feedback (such as vertical acceleration feedback) or off-axis feedback were present in the controller, then figures 26 and 27 could be expanded to include the additional feedback paths. By performing similar block diagram algebra, the effect of being kinematically inconsistent on additional states sums together in the combined transfer function. This is expressed by equation 18 in which the summation occurs over all the n^{th} derivatives of state feedback in which kinematic consistency is not produced. For example, assume the plant, P , represents the transfer function from units of control to altitude. If a disturbance is injected into vertical velocity and integrated into the altitude signal, then the summation of higher order terms would only occur over $n = 2$ if the only other state feedback utilized in the vertical axis is vertical acceleration. If the disturbance was not integrated into the altitude, the summation would occur over $n = 0$ and $n = 2$ (assuming altitude error feedback is present).

$$\frac{f_{tot}}{f} = \frac{1 + P \sum_n s^n C_{y^n}}{1 + CP} = S \underbrace{\left(1 + P \sum_n s^n C_{y^n}\right)}_{\text{Higher Order State Terms}} \quad (18)$$

Comparison between FTIP and Pilot Sweeps:

Another topic worth discussing about FTIP frequency sweeps focuses on how they compare to piloted frequency sweeps. As discussed above, the architecture in DAFCS treats FTIP sweeps as a disturbance for the purposes of disturbance rejection and stability analysis. However, the control induced by an FTIP sweep (along with the AFCS contributions) can be recorded at the input to the mixer (Figure 5). As a result, the FTIP sweep data can be used to generate frequency responses of the airframe alone. While Figure 29 shows that both the piloted and FTIP sweeps produce the same airframe frequency response in regions where the coherence is high, the piloted frequency sweeps typically generate higher quality frequency response data at low frequency.

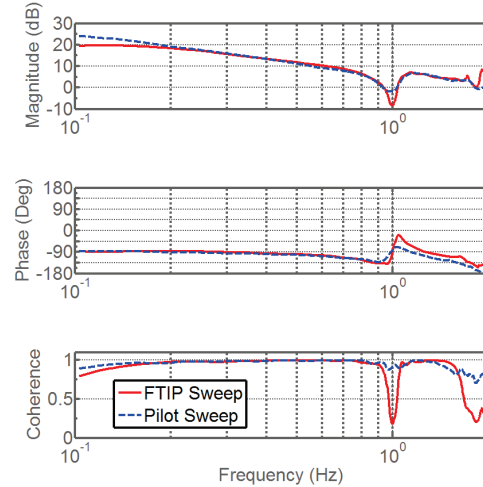
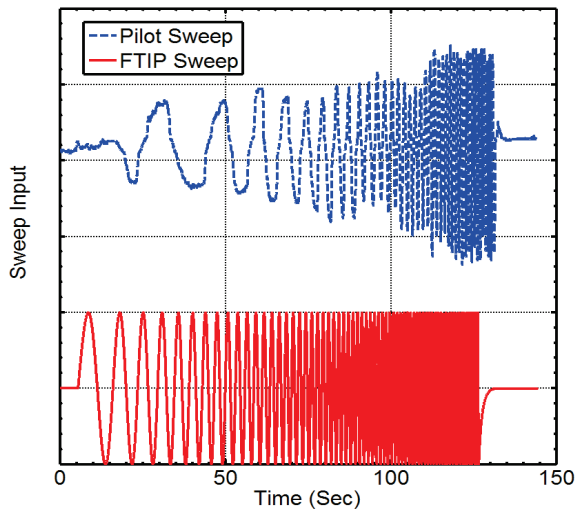


Figure 29: Yaw Rate/Yaw Mixer Frequency Response (Directional Axis – Hover)

The reason for this behavior is that the AFCS is attempting to reject the FTIP sweep (reducing the signal to noise ratio). In addition, when the FTIP sweep excites the rotor-on-rotor drive train mode near 1 Hz, the yaw rate significantly increases. Because the FTIP sweep magnitude is a constant that sums with the other directional axis feedback, the result is that only a small amount of directional axis control is transmitted to the airframe. Because the directional axis response is now dominated by the natural mode rather than the FTIP input, the coherence is significantly reduced in this frequency region. Note that the piloted frequency sweep continued past 1.5 Hz which is why the coherence remained reasonably high up to 2.0 Hz unlike the FTIP. By comparing the two types of frequency sweeps, this example demonstrates two important concepts.

First, regardless of the location of the sweep injection point, the frequency response between two identical signals will be the same (assuming that both of the sweeps excite the input/output signals). However, the choice of input location is important in order to ensure sufficient levels of excitation such that high quality frequency response data can be extracted.

Second, frequency sweep inputs do not need to be perfect sinusoids. While the FTIP sweep input appears to be much cleaner than the piloted input (Figure 30), the pilot sufficiently excited all frequencies within the same range and the frequency response had better coherence in general. In addition, the pilot input had less magnitude than the FTIP sweep at low frequency and still generated better coherence.



**Figure 30: Sweep Input Comparison
(Directional Axis – Hover)**

Conclusions

1. System identification is a powerful tool that can be used to gain physical understanding of the characteristics of a plant. Accurately knowing the predicted consequences of altering control law parameters ahead of time reduces the amount of flight hours spent fine-tuning parameters. As a result, overall program costs can be reduced through the diligent use of system identification.
2. The individuals responsible for performing system identification and linear analysis must have a good understanding of the plant and controller as well as the unique characteristics associated with them. Sometimes results are not intuitive and may lead individuals with insufficient understanding to the wrong conclusions.

3. Based on the purpose and architecture of certain feedback paths, even relatively-large changes in the characteristics of the feedback path may have little impact on the overall stability robustness of a particular axis.
4. The location at which a disturbance is injected into a system can affect the perceived disturbance rejection characteristics. The individuals responsible for designing the test must choose the input location to be representative of the disturbance rejection characteristics relevant to the intent of the analysis. Furthermore, if the intent is ADS-33 spec compliance, the algebra presented in equation 17 (and more generally in equation 18) provides a means of determining the ADS-33 disturbance rejection specifications if there are constraints on the disturbance injection locations.
5. If the augmentation provided by a flight control system occurs at multiple, independent points in the flight controls, then it is necessary to measure directly the location in the flight controls where all of the control transmitted to the aircraft is summed together. This allows for the accurate identification of plant dynamics. In addition, stability margins and disturbance rejection characteristics of the entire control system can be determined with minimal assumptions.
6. Combining pilot-induced and computer-generated frequency sweeps provides high-quality frequency response data. Because of the architecture in DAFCS, computer-generated frequency sweeps had poorer coherence than the piloted sweeps at low frequency because the flight control system was trying to reject the sweeps. In addition, computer-generated sweeps also produced low coherence in frequency regions where natural modes exist. For the purposes of system identification, pilot-induced sweeps generate higher quality frequency response data than computer-generated sweeps within the DAFCS architecture.
7. The many aspects of frequency response analysis in combination with traditional design methods and pilot comments resulted in an aircraft that required minimal in-flight gain tuning to achieve exceptional handling qualities.

References

- [1] Irwin, J.G. and Spano M.S., "MH-47G DAFCS Evolution", American Helicopter Society 67th Annual Forum, Virginia Beach, VA, May 3-5, 2011.
- [2] Tischler, M.B. and Remple R.K., Aircraft and Rotorcraft System Identification, AIAA Education Series, 2006.
- [3] Tischler, M.B. et al., "Handling-Qualities Optimization and Trade-offs in Rotorcraft Flight Control Design", RAeS Rotorcraft Handling Qualities Conference, Liverpool, UK, Nov. 4-6, 2008.
- [4] Miller, D.G., Trim Prediction for Rotorcraft Flight Control, RAeS Rotorcraft Handling Qualities Conference, Liverpool, UK, Nov. 6, 2008.
- [5] Anon., Handling Requirements for Military Rotorcraft, ADS-33E, U.S. Army Aviation and Troop Command, Dec. 1999.
- [6] Kashawlic, B.E. and Irwin, J.G., "MH-47G DAFCS Helicopter Aerial Refueling Control Laws", American Helicopter Society 67th Annual Forum, Virginia Beach, VA, May 3-5, 2011.
- [7] Spano, M.S. and Irwin, J.G., "MH-47G DAFCS Directional-Axis Control Law Development", American Helicopter Society 67th Annual Forum, Virginia Beach, VA, May 3-5, 2011.
- [8] Johnson, C.K. and Kothmann, B.D., "RAH-66 Comanche Flight Test Correlation with Model Predictions: Velocity Stabilization and Altitude Hold Modes", AHS 4th Decennial Specialist's Conference on Aeromechanics, San Francisco, California, January 2004.
- [9] Irwin, J.G., Einthoven, P.G., Miller, D.G., and Blanken, C.L., "ADS-33E Predicted and Assigned Low-Speed Handling Qualities of the CH-47F, with Digital AFCS", American Helicopter Society 63rd Annual Forum, Virginia Beach, VA, May 1-3, 2007.
- [10] Kothmann, B.D. and Armbrust, J., "RAH-66 Comanche Core AFCS Control Law Development: DEMVAL to EMD", American Helicopter Society 58th Annual Forum, Montreal, Canada, June 11-13, 2002.
- [11] Saucedo, R. and Schiring, E.E., Introduction to Continuous and Digital Control Systems, The MacMillan Company, 1968.
- [12] Blanken, C.L. et al., Test Guide for ADS-33E-PRF, US Army Aeroflightdynamics Directorate, July, 2008.